RSC Advances

PAPER

View Article Online
View Journal | View Issue



Cite this: *RSC Adv.*, 2024, **14**, 36576

# Green synthesis, characterization, morphological diversity, and colorectal cancer cytotoxicity of gold nanoparticles†

Sultan Akhtar, *[a] Fatimah Zuhair,[a] Muhammad Nawaz *[b] and Firdos Alam Khan [c]

The synthesis of gold nanoparticles (AuNPs) *via* green methods is advantageous due to their economic viability, reduced environmental pollution, and safety towards human health. According to our best knowledge, there is limited documented research on synthesizing AuNPs using gum Arabic (GA) and cinnamon (CNM) and studying their anticancer activities against colorectal cancer cells. This study presents a simple approach to synthesizing AuNPs using GA and CNM, characterized by advanced analytical techniques, including UV-Vis and FTIR spectroscopies, SEM, EDS, TEM, SAED, Zeta sizer, and Zeta potential. The absorption spectra displayed characteristic bands between 520–530 nm, confirming the successful synthesis of AuNPs. TEM analysis revealed that AuNPs@GA exhibited a spherical shape, while AuNPs@CNM displayed diverse morphologies (*e.g.*, spherical, hexagonal, and diamond shapes) with average sizes of approximately 12 nm and 17 nm, respectively. SEM/EDS data confirmed the presence of AuNPs alongside organic compounds such as carbon, oxygen, and phosphorus. The cytotoxic effects of these AuNPs were evaluated on colorectal cancer cells (HCT-116) and healthy cells (HEK-293) using an MTT assay. Notably, AuNPs@GA resulted in a 43.61% loss in cell viability at the dose of 5 μg mL$^{-1}$, while AuNPs@CNM led to an impressive 80.33% loss. The calculated $IC_{50}$ values were 9.14 μg mL$^{-1}$ for AuNPs@GA and 11.76 μg mL$^{-1}$ for AuNPs@CNM, highlighting the potential of these AuNPs as effective agents in colon cancer treatment. This study not only addresses the lack of research on GA and CNM in NP synthesis but also demonstrates their promising anticancer properties, paving the way for further exploration in cancer therapeutics.

Received 3rd September 2024
Accepted 29th October 2024

DOI: 10.1039/d4ra06340f

rsc.li/rsc-advances



## 1 Introduction

Cancer is a group of diseases that causes uncontrollable and abnormal cell growth leading to tumor formation. Cell proliferation, angiogenesis, and metastasis are the various signaling mechanisms that contribute to cancer development.[1–4] Colorectal cancer (CRC) is one of the most common types of cancer, contributing to significant morbidities and mortalities.[5] Among the different cancers, CRC is the 2nd leading cause of death worldwide. In addition, it is a fatal malignant tumor and has a significant occurrence rate among the age group of 50 and above. Therapies such as chemo, radiation, hormone, immuno, and stem cell transplants are currently the most commonly used treatments for cancer.[6] Chemotherapy is one of the most commonly used therapies for multiple cancer types; however, it involves various cytotoxic agents. The misapplication of chemotherapy causes the initiation of multi-drug resistance and leads to other serious side effects.[1,7–9] This promotes attention to developing and improving other technologies for treating cancer, including nanotechnology.[10]

Nanotechnology is being implemented to transform cancer therapeutic agents and diagnostic techniques. NPs have a significant role in cancer treatment.[11] Synthesizing metal nanoparticles generally utilizes various physical, biological, and chemical methods. Biologically synthesizing NPs involves the utilization of several microorganisms and their enzymes and plant extractions, known as green synthesis.[8,12,13] Biological techniques have several advantages such as cost-effectiveness and eco-friendliness. Moreover, the green synthesis method does not include high pressures, energy, high temperatures, or hazardous chemicals.[8,14–18] Metal nanoparticles manufactured using biomolecules from biological sources exhibit unique physiochemical characteristics, such as affordable nanosynthesis, broad optical characteristics, surface functionality, and

[a]*Department of Biophysics Research, Institute for Research and Medical Consultations (IRMC), Imam Abdulrahman Bin Faisal University, Dammam, 31441, Saudi Arabia. E-mail: suakhtar@iau.edu.sa*

[b]*Department of Nano-Medicine Research, Institute for Research and Medical Consultations (IRMC), Imam Abdulrahman Bin Faisal University, Dammam, 31441, Saudi Arabia. E-mail: mnnmuhammad@iau.edu.sa*

[c]*Department of Stem Cell Research, Institute for Research and Medical Consultations (IRMC), Imam Abdulrahman Bin Faisal University, Dammam, 31441, Saudi Arabia*

† Electronic supplementary information (ESI) available. See DOI: https://doi.org/10.1039/d4ra06340f

a high surface-to-volume ratio, providing an innovative chance for cancer treatment. Metal NPs were extensively used in developing antibacterial, antifungal, antiviral, anticancer technologies, biosensors, drug delivery, chronic disease diagnostics, gene therapy agents, *etc.*[19–25] Accordingly, a growing area of study is the synthesis of NPs using the green method, especially metal NPs. It provides several benefits such as the absence of harmful solvents and reagents, waste production, and inhibiting the generation of byproducts when preparing metal NPs. Further, it stimulates the use of renewable natural resources.[26]

The synthesis of NPs *via* green methods is advantageous due to their economic viability, reduced environmental pollution, and safety for human health. In biomedical applications, gold NPs are among the most widely used metallic NPs as they are compatible with the biological system, have tiny size, lower toxicity, simplified surface modification, locus-specific target locations used in cancer treatment, and high functionality.[24,27–31]

Gum Arabic (GA) can function as a stabilizing and reducing agent, gathered from Acacia Senegal trees.[32–34] It is a polymeric compound with the chemical formula [$C_{15}H_{20}NNaO_4$] and made of long chains of glycoprotein and polysaccharides as well as Mg, K, and Ca salts.[34,35] GA atoms are composed of COOH and $NH_2$ groups. During the preparation, these groups are attached to the surface of the NPs, hence improving the colloidal stability by producing a repulsion force among the NPs.[34,36] Smaller AuNPs with excellent properties and high stability can be provided *via* GA coating that showed insignificant adverse effects.[31,34,37–39] On the other hand, *Cinnamomum cassia* (Chinese cinnamon) (CNM) has many therapeutic characteristics, it was used as an anti-bacterial, anti-inflammatory, anticancer, and antioxidant agent.[40]

Various studies demonstrated that the cytotoxic efficacy of nanoparticles relies on their physiochemical characteristics, leading to various effects on different types of cancer and healthy cells.[41] Thus, it is crucial to investigate the characteristics of the NPs and study their anticancer activities against different cell lines. The present study presents a simple approach to synthesizing AuNPs using GA and CNM as reducing and stabilizing agents, characterized by advanced analytical techniques, including SEM, EDS, TEM, SAED, UV-Vis, and FTIR spectroscopies, Zeta sizer, and Zeta potential of the synthesized AuNPs@GA and AuNPs@CNM. The anti-cancer potency of these synthesized AuNPs was investigated against cancer cells (HCT-116) and normal cells (HEK-293). The cytotoxicity of the prepared AuNPs@GA and AuNPs@CNM was investigated at different concentrations using MTT assay, confocal, optical, and electron microscopy techniques. This study not only addresses the synthesis of NPs using gum Arabic and cinnamon but also evaluates their anticancer properties, aiming to explore improved cancer therapeutics.

# 2 Materials and methods

## 2.1 Materials

Gold (III) chloride trihydrate ($HAuCl_4 \cdot 3H_2O$, 99.9%) is obtained from Sigma Aldrich. Gum Arabic (GA) is utilized to prepare GA solution and cinnamon (CNM) powder was obtained from a local market in Saudi Arabia.

## 2.2 Synthesis of AuNPs

The preparation of GA solution was done by adding 0.4 g of GA in 25 mL of DI water and was left to stir for 20 minutes. For the CNM solution, 2.5 g of CNM powder was added to 100 mL of DI water. The solution was then heated on a hot plate at 45 °C for 20 min. After cooling, the solution was filtered to obtain CNM extract. The preparation of the $HAuCl_4$ solution was done by adding 0.0287 g of $HAuCl_4$ to 66 mL of DI water. To synthesize AuNPs@GA, 3 mL of both $HAuCl_4$ and GA solutions were mixed and then heated again on a hot plate for 15 min. Similarly, for AuNPs@CNM, 3 mL of both CNM and $HAuCl_4$ solutions were added to a flask and heated at 45 °C for 15 min. A detailed synthesis of AuNPs using GA and CNM is demonstrated in Fig. 1.

## 2.3 Characterization of AuNPs

The structure and morphology of AuNPs@GA and AuNPs@CNM were investigated by (TEM), (SAED) (FEI TEM, Morgagni 268, Czech Republic), and (SEM/EDS) (TESCAN, Vega 3 SEM, Czech Republic).[42–44] EDS was used to verify the presence of different elements in the synthesized AuNPs. Also, SEM was utilized to find the morphology of HCT-116 and HEK-293 after treatment for 24 h. TEM sample preparation was performed by placing a drop of AuNPs dispersion of each sample onto TEM grids. The grids were then inserted into TEM to obtain images of the NPs. The size of AuNPs was determined by measuring 150 particles for each sample. For SEM/EDS, a few drops from each sample were placed onto metallic stubs having double-sided carbon tape.

The prepared AuNPs were characterized by a UV-vis spectrometer (JASCO V-750 Inc., Helsinki, Finland) to find the absorption properties and to confirm the formation of AuNPs@GA and AuNPs@CNM. Fourier transform infrared (FTIR) spectroscopy (PerkinElmer spectrometer, Boston, Massachusetts, United States (USA)). The spectral data was measured in the range of 4000 to 400 $cm^{-1}$ wavenumber. The size distribution and surface charge of the NPs are crucial for assessing stability and interaction with biological systems. Dynamic light scattering (DLS) instrument (Malvern ZETASIZER NANO, United Kingdom (UK)) was carried out to find out the particle size distribution, particle mean size, zeta potential, and polydispersity index (PDI) of the synthesized AuNPs@GA and AuNPs@CNM specimens. The figures of DLS, Zeta sizer, and Zeta potential are displayed in ESI.†

## 2.4 Anticancer activity of the AuNPs

The anticancer activity of the two prepared NPs specimens was determined by using an MTT assay. The HCT-116 and HEK-293 cell lines were obtained from ATCC, Virginia, USA. The preparation of cells for the MTT assay was described in our previous report.[45] In summary, we cultured the cells in standard media in a $CO_2$ incubator. Different concentrations of the NPs (5, 10, 20, 40, and 60 μg $mL^{-1}$) were used to treat the cells *e.g.*, 24 h

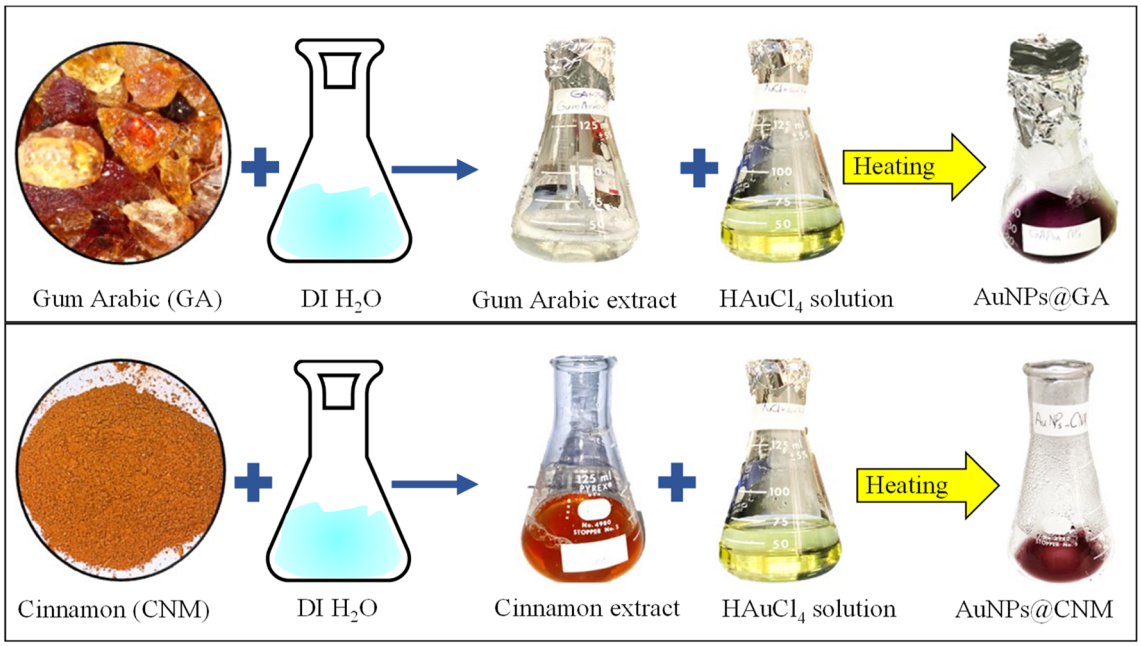


Fig. 1 A schematic diagram showing the synthesis process of AuNPs@GA and AuNPs@CNM using gum Arabic (GA) and cinnamon (CNM).

incubation at 37 °C for both cancer cell lines. Then, the media was replaced with MTT solution and incubated the plates again for 4 h at 37 °C. The cell viability was determined by a multimode reader (BioTeK, Synergy, $NEO_2$, multimode reader, USA). The cell viability (C. V.) of AuNPs@GA and AuNPs@CNM specimens were calculated using the following relation (1):

$$\text{C.V.}(\%) = \left(\frac{(\rho)_{\text{AuNPs}}}{(\rho)_{\text{control}}}\right) \times 100 \quad (1)$$

where $\rho_{\text{control}}$ and $\rho_{\text{AuNPs}}$ are the optical densities of the control and treated cells, respectively.

### 2.5 Imaging by light microscopy

The cells were observed under light microscopy (LM) to identify the morphological changes that occurred in the viability of the cells after treatment with gold NPs. A light microscope (Nikon Eclipse TS100, Japan) was used to obtain images of different concentrations (5 and 60 μg $mL^{-1}$) of controlled and treated cells (HCT-116 and HEK-393).

### 2.6 Sample preparation of cells for LM and SEM

To observe the morphological changes, the control, and treated cells of HCT-116 and HEK-293 were investigated under (LM) and (SEM). To prepare the samples for LM and SEM examinations, 20 000 cells were counted and placed in a media into a 6-well plate. Then, they were incubated for 24 h with 60 μg $mL^{-1}$ of AuNPs@GA and AuNPs@CNM specimens. The cells were washed with a buffer and fixed with 3% glutaraldehyde for 1 h. After the first fixation, the cells were washed again three times with buffer and fixed with secondary fixative: $OsO_3$ (osmium tetroxide) for 2 h at 4 °C. Graded ethanol was used for sample dehydration. Sample infiltration was done with propylene oxide and resin solution under four different ratios. On the completion of infiltration, the samples were incubated overnight. Thereafter, fresh resin was added to the embedding molds and kept at 60 °C for 24 h. An Ultramicrotomy machine (LEICA EM UC7, Japan) was used to prepare the sections with a glass knife. The toluidine blue stain was used to stain the sections and then investigated under an LM (Nikon ECLIPSE H550L, Japan). For SEM, 3% of glutaraldehyde solution was used for cell fixation, washed with PBS, and dehydrated by graded ethanol (30–100%) for 30 min each. After dehydration, the samples were freeze-dried using a critical drying machine operated under $CO_2$ gas. Finally, the samples were mounted onto an SEM holder, sputter coated with gold, and examined under SEM.

### 2.7 Morphology of the cells by DAPI staining

The DNA structure of cancer cells can be investigated by DAPI stain. HCT-116 and HEK-393 cells were distributed into groups: (1) a control with no AuNPs and (2) a treated with 60 μg $mL^{-1}$ of AuNPs@GA and AuNPs@CNM for 24 hours of treatment. 4% paraformaldehyde was introduced, then PBS was added in addition to treating with DAPI (20 μL $mL^{-1}$). After that, the cells were washed with PBS and examined under a confocal microscope.

### 2.8 Statistical analysis

The data are presented as mean (±) standard deviation (SD) obtained from triplicates. The findings of this study were analyzed by IBM SPSS software for statistical analysis. The *p*-value is calculated where $p < 0.05$ is considered as significant.

# 3 Results and discussion

## 3.1 Analysis of synthesized AuNPs

The AuNPs were synthesized using two plant extracts: GA and CNM. GA and CNM functioned as stabilizing agents to protect gold nanoparticles from aggregation. After exposing the samples to heat, the color of the reaction solutions gradually shifted from a bright yellow solution to a purplish red, demonstrating the synthesis of AuNPs Fig. 1.[46] Changing the color indicates the oscillation of the conduction band electrons of the NPs.[34,47,48] It demonstrates the reduction of gold$^{3+}$ to gold$^{0}$, confirming the formation of AuNPs.[47,49] The coating with GA made the particles apart from each other; thus, increasing the number of single particles.[34] The GA network's COOH groups hold the NPs *via* hydrogen bonding, which aids the NPs to remain separate and stable.[50] The main constituent of cinnamon that reduces $HAuCl_4$ is *trans*-cinnamaldehyde, which also contributed to the color change.[47,49]

The structure of prepared AuNPs was determined by TEM, SAED, and SEM/EDS. The TEM results analysis is shown in Fig. 2. The synthesized gold nanoparticles exhibited several morphologies, such as spherical, diamond, hexagonal, and

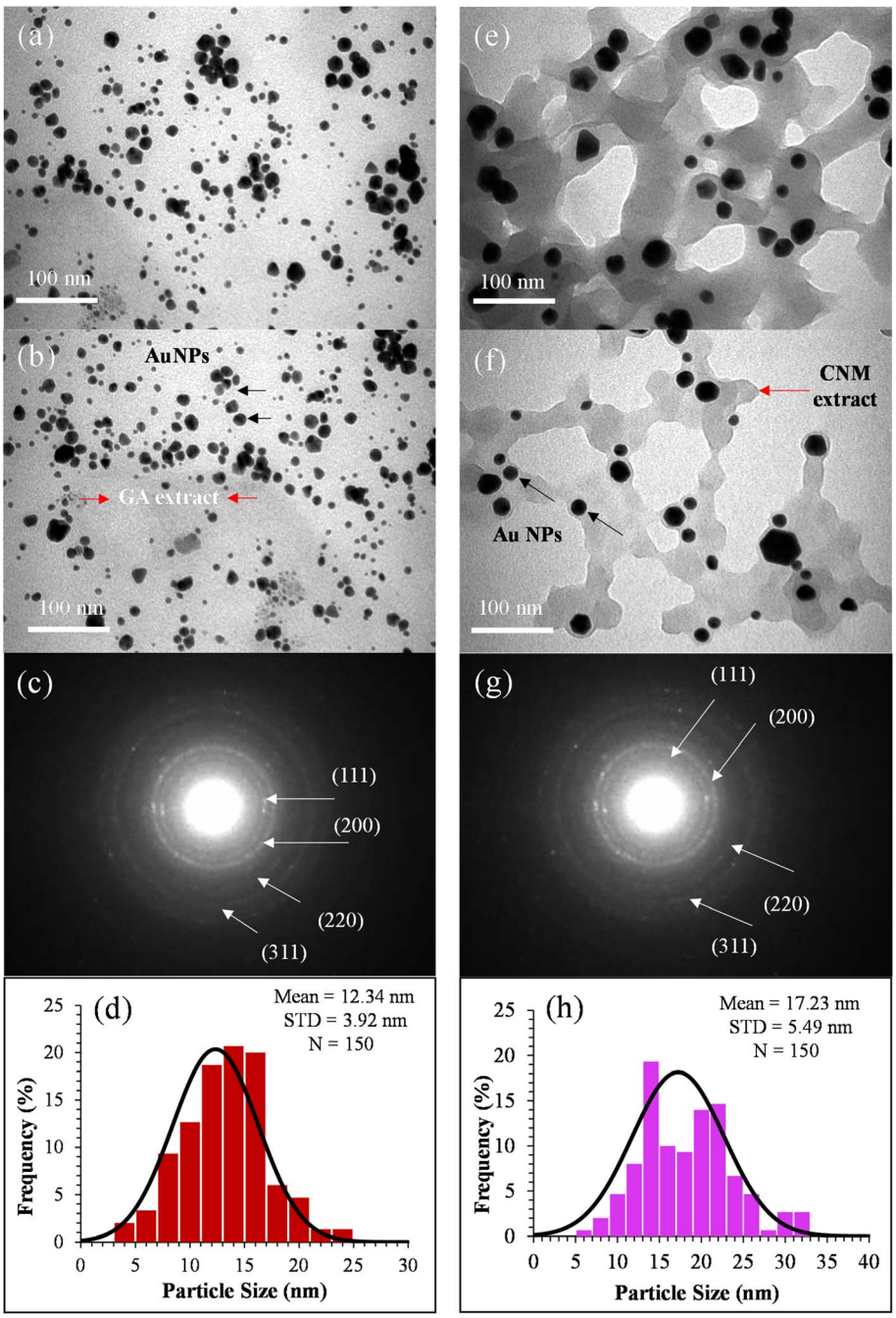


Fig. 2 TEM images, SAED pattern, and size histogram of AuNPs@GA (a–d) and AuNPs@CNM (e–h).

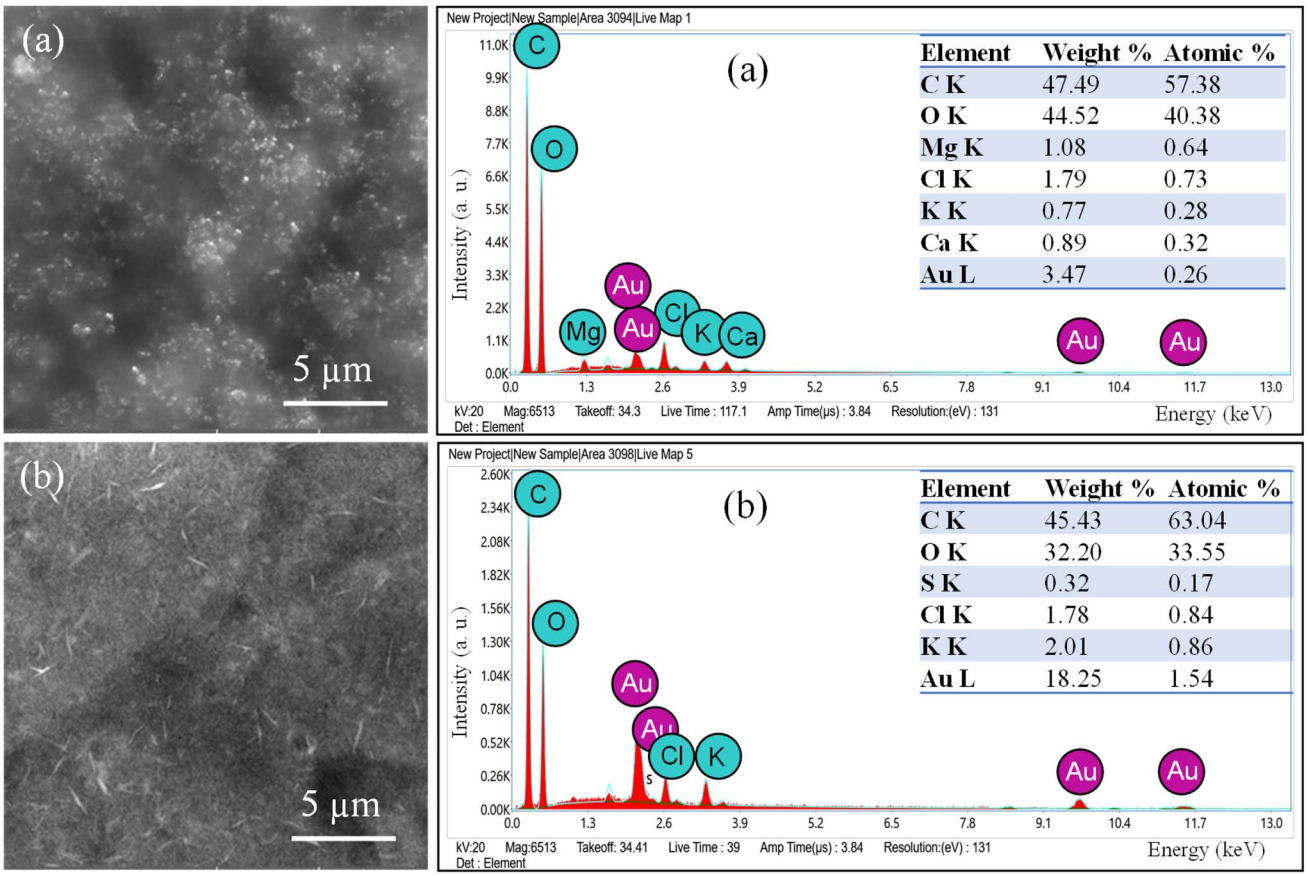


Fig. 3 SEM images, EDS spectra, and chemical composition of (a) AuNPs@GA and (b) AuNPs@CNM specimens.

pentagonal morphologies, and the average size was about 12 and 17 nm.[51] TEM results of AuNPs@GA showed that the morphology of the nanoparticles was predominantly spherical and these findings agreed with the earlier studies.[34,52] On the contrary, it also found that the anisotropy of the AuNPs@CNM has various shapes, such as spherical, triangular, and hexagonal, showing non-symmetric AuNPs, that is consistent with previous studies.[53] The presence of chemicals in cinnamon formed a film on the surface of NPs, which prevented their agglomeration. The SAED patterns of the synthesized AuNPs@GA and AuNPs@CNM are shown in Fig. 2(c and g). The patterns of AuNPs@GA and AuNPs@CNM exhibited a ring-shaped pattern corresponding to (111), (200), (220), and (311), showing a crystalline nature. This signifies that the organic molecules can synthesize and stabilize AuNPs in an aqueous medium.[54] Furthermore, SEM/EDS was conducted to identify the external shape, elemental composition, and elemental distribution. Fig. 3 demonstrates SEM results, EDS spectra, elemental composition, and distribution. The EDS spectrum of AuNPs@GA demonstrated the following elements: C, O, Mg, Cl, K, Ca, and Au. The EDS spectrum of the AuNPs@CNM specimen exhibited O, S, Cl, K, and Au. The appearance of Au peaks in both spectra confirms the successful preparation of AuNPs. The peaks of C, O, Mg, Cl, K, and Ca in the spectra indicate the presence of organic agents of gum Arabic and cinnamon around the AuNPs. EDS mapping was conducted further to confirm the elements found in the EDS analysis as well as to find out their atomic distribution in the AuNPs@GA and AuNPs@CNM (Fig. 4). EDX mapping images demonstrate the uniform distribution of gold in the background of carbon and oxygen. A uniform distribution of the C, O, Cl, and Au can be seen in the mappings, highlighting the existence of expected elements in the prepared specimens. The mapping of the AuNPs@GA and AuNPs@CNM also revealed that the AuNPs are successfully coated with either gum Arabic or cinnamon. In summary, SEM examination, EDS elemental and EDS mapping analyses altogether confirmed the successful preparation of AuNPs@GA and AuNPs@CNM *via* green synthesis using plant extracts.

The absorption properties of the green synthesized NPs (AuNPs@GA) and (AuNPs@CNM) were evaluated using UV-visible spectroscopy (see Fig. 5a). The surface plasmon resonance (SPR) band exhibits a red shift with an increase in particle size. In contrast, the aggregation of colloidal gold results in a decrease in the intensity of the main peak and produces a long tail on the longer-wavelength side of the peak.[55] The UV-Vis spectroscopy data showed the characteristic (SPR) absorption bands for AuNPs@GA and AuNPs@CNM specimens. The emergence of the band in the UV-Vis spectra at 520–530 nm confirmed the successful synthesis of AuNPs@GA and AuNPs@CNM,[38] which corresponded with the color conversion from light yellow to transparent purplish red indicating the presence of NPs in the solution.[36,56] The UV-Vis absorption

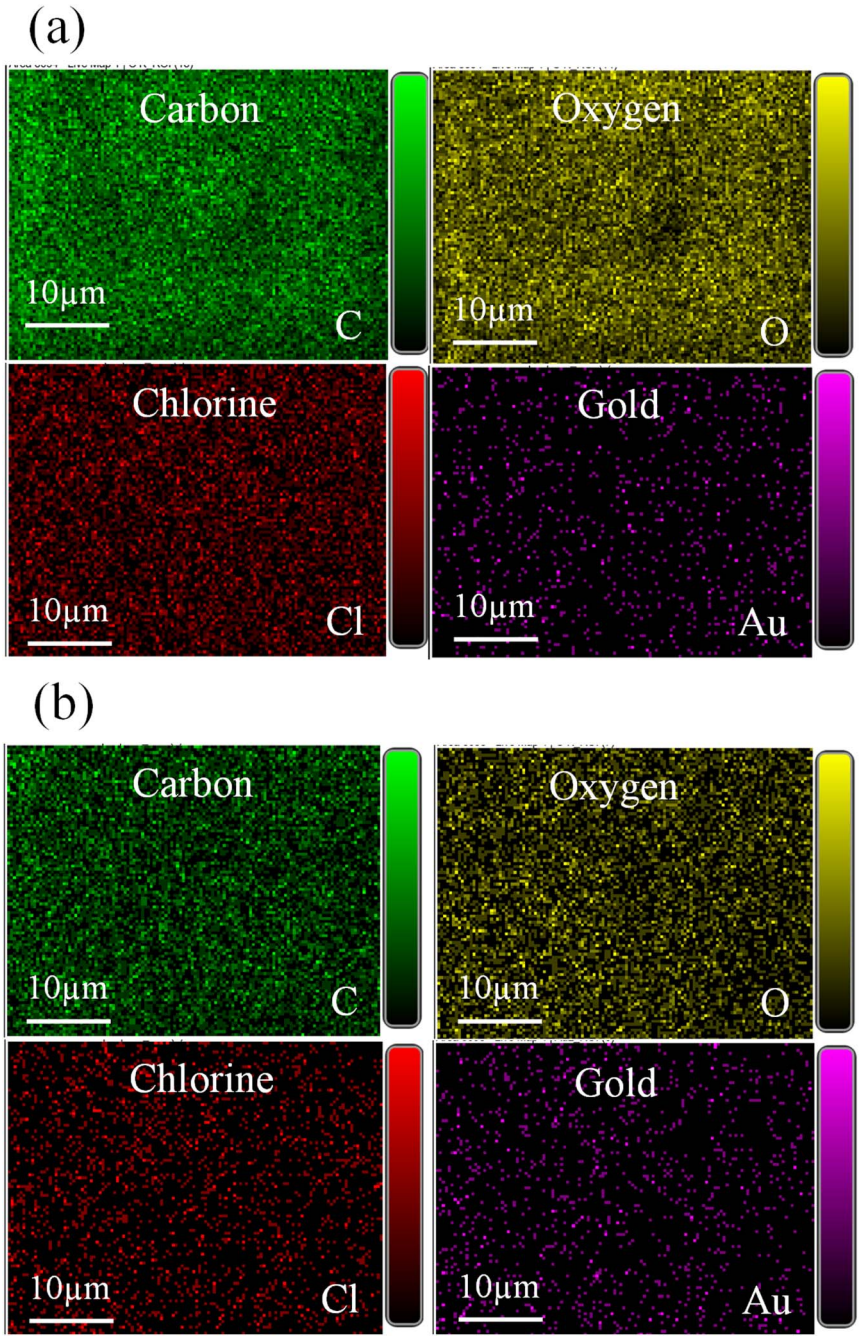


Fig. 4 EDS elemental mapping images of (a) AuNPs@GA and (b) AuNPs@CNM specimens.

spectra showed no significant change, with a slight shift of the characteristic absorption band. The finding of the AuNPs@GA absorption peak (525 nm) with 40 mg of GA matches the finding as reported by other authors (Qureshi *et al.*, 2022).[57] The key constituent found in cinnamon, *trans*-cinnamaldehyde, plays a crucial role in reducing the $HAuCl_4$ in an aqueous solution, resulting in the formation of a wine-red solution containing AuNPs.[56] According to one study, results indicated that a higher temperature led to accelerating the formation rate of AuNPs, while the characteristic absorption band showed no noticeable shift, suggesting that the resulting AuNPs were of similar size across the temperature range studied. At a gum Arabic concentration of just 1 mg $mL^{-1}$, the resulting Au solution turned purple-red, and its absorption band weakened, broadened, and shifted toward the red. This implied that the gum Arabic concentration was too low to fully reduce all Au ions and provide sufficient stabilization for AuNPs. As the gum Arabic concentration ranged from 5 to 20 mg $mL^{-1}$, the characteristic absorption band of the resulting Au solutions exhibited a slight red shift with the increase in gum Arabic concentration. The change in optical properties may be attributed to differences in particle size and size distribution.[51] Moreover, a study

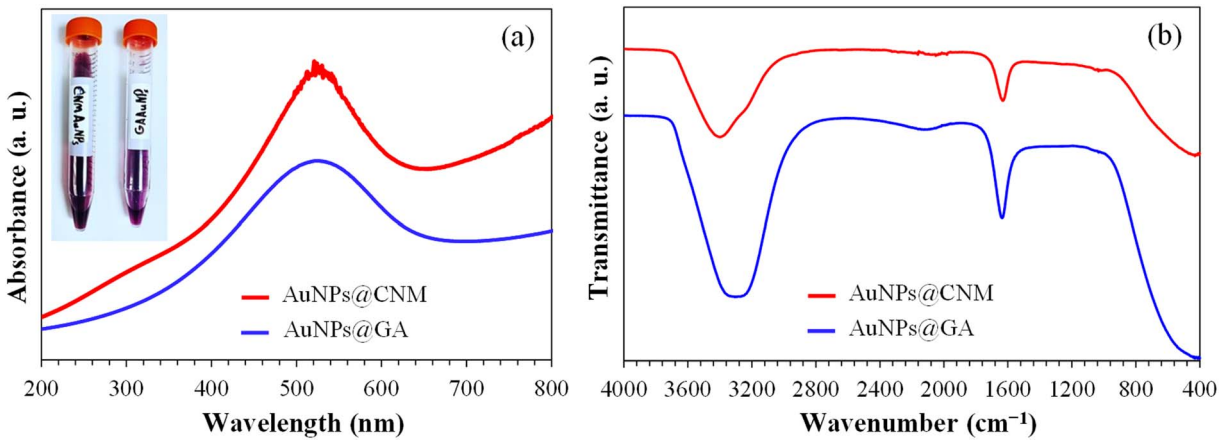


Fig. 5 (a) UV-Vis absorption spectra of the prepared AuNPs@GA and AuNPs@CNM, (b) FTIR spectra of the prepared AuNPs@GA and AuNPs@CNM.

mentioned the effectiveness of AuNPs formation improves with higher concentrations of gum while maintaining a fixed concentration of $HAuCl_4$. However, a further increase in the gum concentration leads to a decrease in peak intensity and a shift of the peaks toward longer wavelengths. It can be noted that the strong absorption band intensifies with an increase in concentration and reaction time.[55] In addition, it is widely recognized that the optical absorption spectra of metal NPs exhibit longer wavelengths as particle size increases.[58]

Earlier, TEM observation confirmed that both Gum Arabic and cinnamon were capable of wrapping the AuNPs and protecting them from large aggregation, particularly for AuNPs@CNM where the NPs were appeared as individuals and clearly distinguished by their dark contrast compared to cinnamon extraction. The carboxyl and hydroxyl groups of gum Arabic and cinnamon capped the NPs through hydrogen bonding, allowing them to remain apart and offering NPs stability. Fig. 5b presents the FTIR spectra of AuNPs@GA and AuNPs@CNM. The recorded bands appeared at about 3000–3400, 2120, 1630, and 1049 $cm^{-1}$. The peaks observed at 3000–3400 $cm^{-1}$ correspond to O–H stretching. The interaction between green extracts and AuNPs *via* hydroxyl and carbonyl groups exhibited a stretching vibration of the hydroxyl group at 3400 $cm^{-1}$. 2120 $cm^{-1}$ represents the stretching vibration of C–H bonds. The peaks at 1630 $cm^{-1}$ showed C=C stretching vibrations. Moreover, both spectra displayed the primary characteristic peaks of GA and CNM at 1049 $cm^{-1}$ corresponding to the C–O stretch.[59] The similarity between the spectra confirmed the presence of green extracts on the surface of AuNPs. Consequently, the strong stability of the AuNPs is due to the effective protection provided by GA and CNM on their surface.[38] The results showed that both hydroxyl and carboxyl groups played a role in the synthesis and stabilization of AuNPs. The formation of AuNPs occurs in two steps. Initially, the gum containing hydroxyl functional groups is oxidized to produce carbonyl functional groups, and concurrently, Au ions are reduced to Au

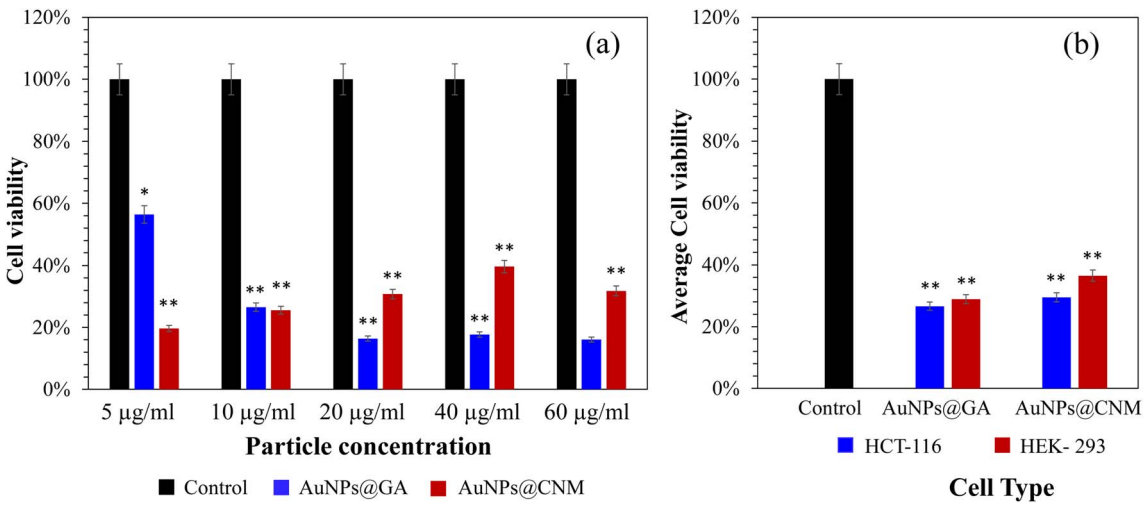


Fig. 6 (a) *In vitro* cytotoxic efficacy of AuNPs on HCT-116 cells under different concentrations (5, 10, 20, 40, and 60 µg $mL^{-1}$). (a) Cell viability of control and AuNPs treated HCT-116 cells; (b) average cell viability of control, HCT-116, and HEK-293 cells. The cell viability of post-24 h treatment. *$p < 0.05$; **$p < 0.01$.

atoms. During the next step, the oxygen atom found in the carbonyl and hydroxyl functional groups contributes to creating a layer that prevents the aggregation of NPs, as it strongly interacts with the AuNPs.[55]

The Zeta potential of AuNPs@GA and AuNPs@CNM are presented in ESI (see Fig. S1).† The potential of AuNPs@GA and AuNPs@CNM was recorded at −19.1 mV (ref. 36) and −8.37 mV, respectively. The Zeta potential results showed that AuNPs@GA have higher dispersion stability than AuNPs@CNM. A high negative value of potential indicates that the particles can repel each other and maintain excellent stability over time by preventing agglomeration. The average particle size of AuNPs@GA was observed at 68.66 ± 8.85 nm with (PDI: 0.84), and for AuNPs@CNM, it was 359.4 nm (PDI: 0.71) (see Fig. S2†). The discrepancy between the particle sizes observed in TEM and DLS can be attributed to TEM capturing the diameter of individual particles. In contrast, DLS measures the hydrodynamic radius of the NPs, DLS also considers the capping shell, thereby offering insights into the size of the entire conjugate as demonstrated in Fig. S3.† In suspensions of small AuNPs, the quantity of saccharide molecules per particle is elevated resulting in a hydrodynamic size from DLS that is larger than the size determined by TEM. Additionally, DLS analyzes NPs in a liquid solution and is consequently influenced by aggregation or accumulation. The PDI was also measured to determine whether the NP size distribution is polydisperse or monodisperse. The PDI value of AuNPs@GA and AuNPs@CNM was observed at 0.84 and 0.71, respectively, indicating high poly-dispersibility of the NPs, which can be ascribed to the existence of a diverse range of particles.[55,60] Pooja *et al.* showed that the gum-stabilized AuNPs had an average hydrodynamic diameter of 41 ± 3.78 nm. The nanoparticles exhibited high polydispersity (0.35–0.6), which can be due to the presence of a diverse range of particles. The high negative surface potential showed that the nanoparticles have strong stability in the existence of gum molecules.[61]

### 3.2 MTT assay for cytotoxicity of AuNPs

The effect of AuNPs@GA and AuNPs@CNM on the cancer cell lines (HCT-116) was investigated. Consistent with previous studies, the MTT cell proliferation assay confirmed that AuNPs exhibited a cytotoxic effect against cancerous cells.[8,62] The cancer cell line, HCT-116 loses approximately 43.61% of its viability, after treatment with 5 μg mL$^{-1}$ AuNPs@GA. On the

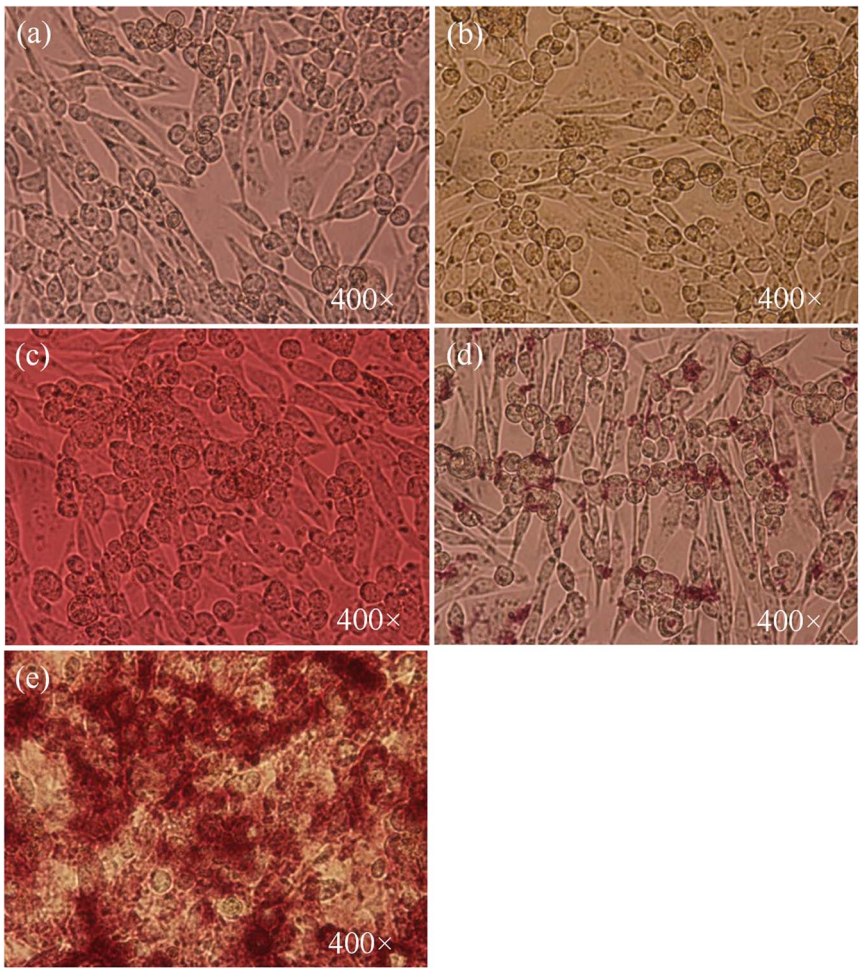


Fig. 7 Cell morphology of HCT-116 cells. (a) Control, treated for 24 h with (b) 5 μg mL$^{-1}$ AuNPs@GA, (c) 60 μg mL$^{-1}$ AuNPs@GA, (d) 5 μg mL$^{-1}$ AuNPs@CNM, and (e) 60 μg mL$^{-1}$ AuNPs@CNM.

other hand, treatment with 5 μg $mL^{-1}$ AuNPs@CNM led to about 80.33% loss in cell viability for HCT-116 as shown in Fig. 6(a). SEM analysis later confirmed the presence of apoptotic bodies in the treated HCT-116 cells. Also, the DAPI-stained cells number was notably reduced, and apoptotic bodies were formed with the existence of AuNPs as compared to control cells (Fig. 11). Several studies also reported that the treatment of green synthesized AuNPs has induced potential anticancer activity.[29,63–65] Aldawsari *et al.* reported that AuNPs@GA exhibited cytotoxicity against MCF-7.[65] Similarly, AuNPs synthesized by Parsley leaf extract demonstrated cytotoxicity against HCT-116 at a low concentration; this cytotoxic effect might occur due to the free radicals produced by NPs. Additionally, the small size of the NPs led to the damage of the membranes of cancer cells, as shown in Fig. 9, which is consistent with a research finding.[66] The treatments of AuNPs have different actions against various types of cancer cells. Both AuNPs@GA and AuNPs@CNM were not sensitive to concentration. Some other studies revealed that small-sized nanoparticles resulted in a better cytotoxic effect than larger nanoparticles. This outcome could be justified by the results of these studies.[57,67,68] Steckiewicz *et al.* revealed that the cytotoxic activity of AuNPs is affected by the size, morphology, concentration, incubating time, preparing technique, treated cell line, and surface functionalization.[69] The $IC_{50}$ values for AuNPs@GA and AuNPs@CNM on HCT-116 were calculated at about 9.14 and 11.76 μg $mL^{-1}$, respectively. It can be seen that the treatment of AuNPs@GA showed better inhibitory action on HCT-116 than AuNPs@CNM; this could be because of the small nanoparticle size of AuNP-GA. Also, a study showed that smaller gold nanoparticles have better membrane penetration than large-sized Au nanoparticles.[70] Fig. 7 and 8 represent the light microscopy observations of cancer and healthy cell lines after treating them with different concentrations of AuNPs@GA and AuNPs@CNM. The morphology of HCT-116 cancer cells is significantly affected even by lower AuNPs concentrations and the number of cells decreased compared to the control (Fig. 7(a)). Nonetheless, Fig. 8 showed that HEK-293 normal cells were affected at a high concentration. In addition to the cytotoxicity study of NPs on the cell line (HCT-116), the internal structure, cell morphology, and apoptotic effects on control and treated cells (HCT-116) were studied using LM, SEM, and laser confocal microscopy (Fig. 9–11). Notably, HCT-116 cell lines were selected to highlight further the effects of NPs on cancerous cells. For

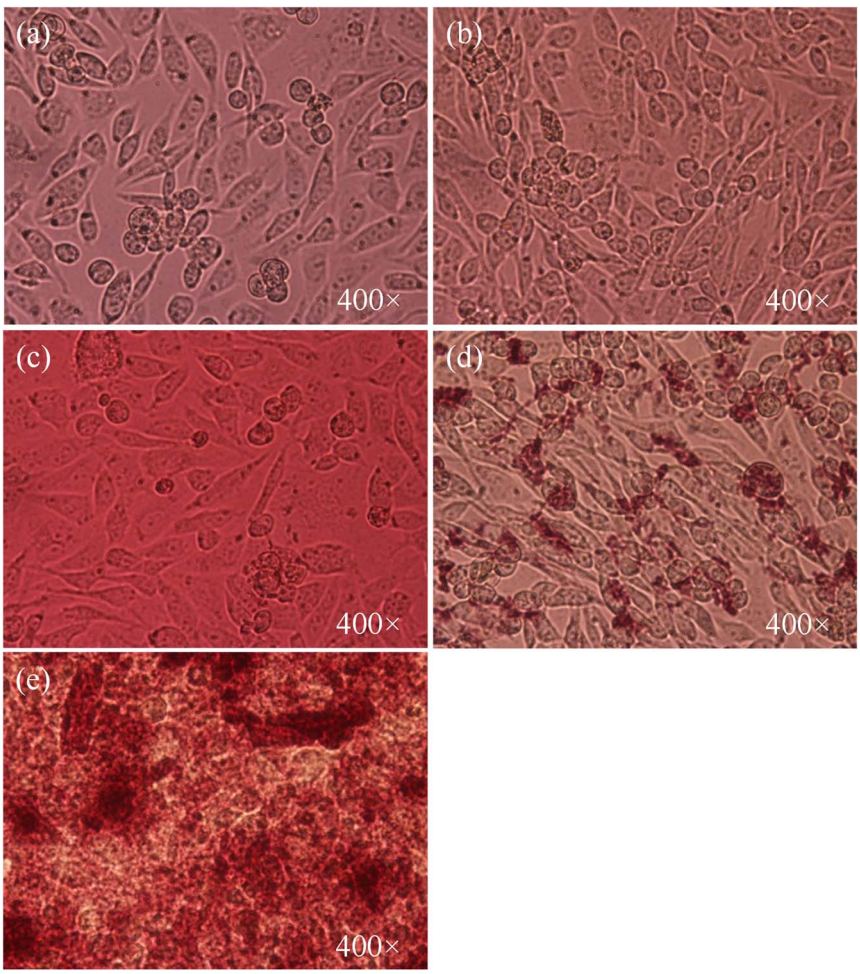


Fig. 8 Cell morphology of HEK-293 cells. (a) Control, treated for 24 h with (b) 10 μg $mL^{-1}$ AuNPs@GA, (c) 60 μg $mL^{-1}$ AuNPs@GA, (d) 10 μg $mL^{-1}$ AuNPs@CNM, and (e) 60 μg $mL^{-1}$ AuNPs@CNM.

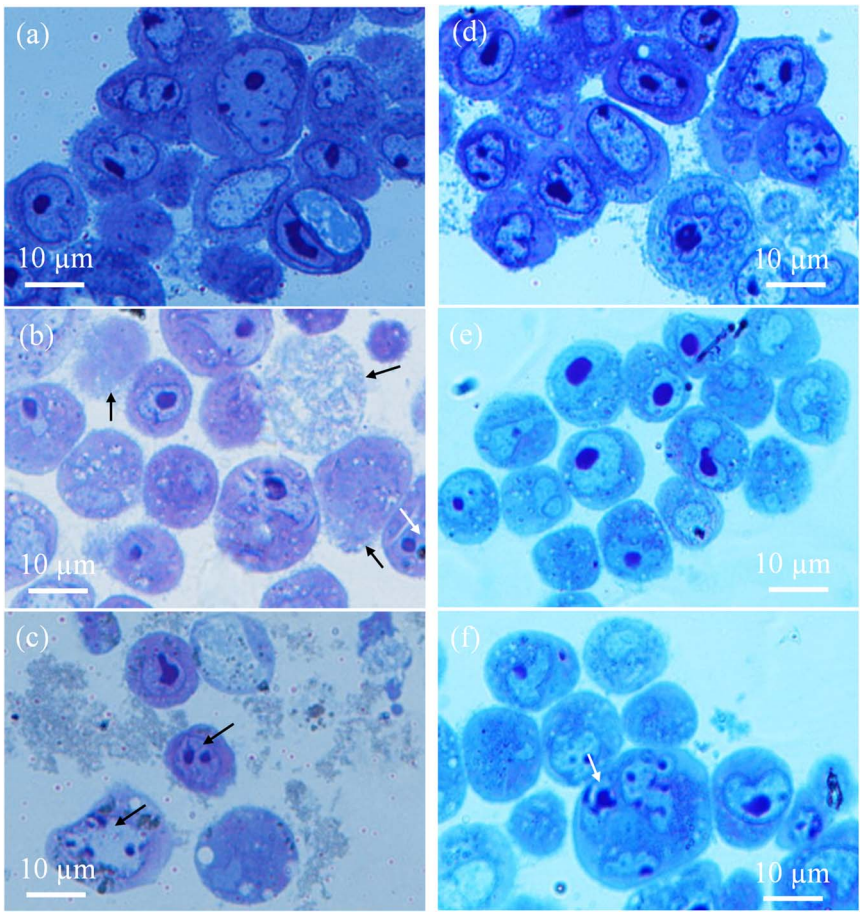


Fig. 9 Cell morphology: light microscopy micrographs of ultramicrotomy prepared control, and treated HCT-116 (left panel) and HEK-293 cells (right panel). (a) Control, treated for 24 h with (b) 60 μg $mL^{-1}$ AuNPs@GA and (c) 60 μg $mL^{-1}$ AuNPs@CNM. Light microscopy images of (d) control and treated HEK-293 cells with (e) 60 μg $mL^{-1}$ AuNPs@GA and (f) 60 μg $mL^{-1}$ AuNPs@CNM. Loss of cell features is highlighted with black arrows while white arrows show nuclear fragmentation. All scale bars are 10 μm.

comparison, the healthy cells (HEK-293) were also included in this analysis. There are reports where gold nanoparticles were tested on both cancer and normal cells to understand the safety of the gold nanoparticles. In one study, the treatment of gold nanoparticles showed a profound anticancer effect on the prostrate colon and lung cells and a less pronounced impact on normal colon cells.[71] In another study, the treatment of gold nanoparticles showed an anticancer effect on human gastric adenocarcinoma, where the treatment on normal mammalian cell lines, such as RAW264.7 macrophages, normal human dermal fibroblasts (NHDF) cells, and human embryonic kidney 293 (HEK-293) showed less cytotoxicity with compared to cancer cells.[72] Additionally, the treatment of gold nanoparticles showed more cytotoxicity to liver cancer cells than normal human cells.[73] In another study, the treatment of gold nanorods showed cytotoxicity against both prostate cancer and normal prostate cells.[74]

### 3.3 Morphological and structural analyses of the chemically fixed cells

After the incubation with AuNPs@GA and AuNPs@CNM for 24 h, the treated cells showed abnormalities in morphology, such as shrinking of the cells, cell membrane swelling, formation of apoptotic bodies, chromatin condensation, and fragmentation, as illustrated in Fig. 9 (light microscopy observation). These cellular alterations can be explained by the entrance of AuNPs@GA and AuNPs@CNM into the cells by endocytosis, micropinocytosis, *etc.* afterward, releasing reactive oxygen species (ROS) which destroy the potency of the mitochondrial membrane activating the apoptotic pathway leading to cell death.[75,76] Similarly, Han *et al.* reported that AuNPs exhibited high levels of ROS formation in HCT-116 cells.[29] Also, their findings indicated that mitochondrial membrane potential was damaged after AuNPs treatment. Moreover, Mkandawire *et al.* showed that gold nanoparticles led to exterior mitochondrial membrane rupture and, therefore, induced apoptosis in MCF-7 cells.[77] In addition, the surface morphology of the chemically fixed cells (HCT-116 and HEK-293) was examined by (SEM) to further highlight the effects of NPs on treated cells. SEM results of control and treated cells are shown in Fig. 10. The normal cells, HCT-116 and HEK-293 showed uniform morphology while treated cells of HCT-116 displayed abnormalities in morphology (shrinking, membrane swelling, apoptotic formation, and fragmentation), confirming the

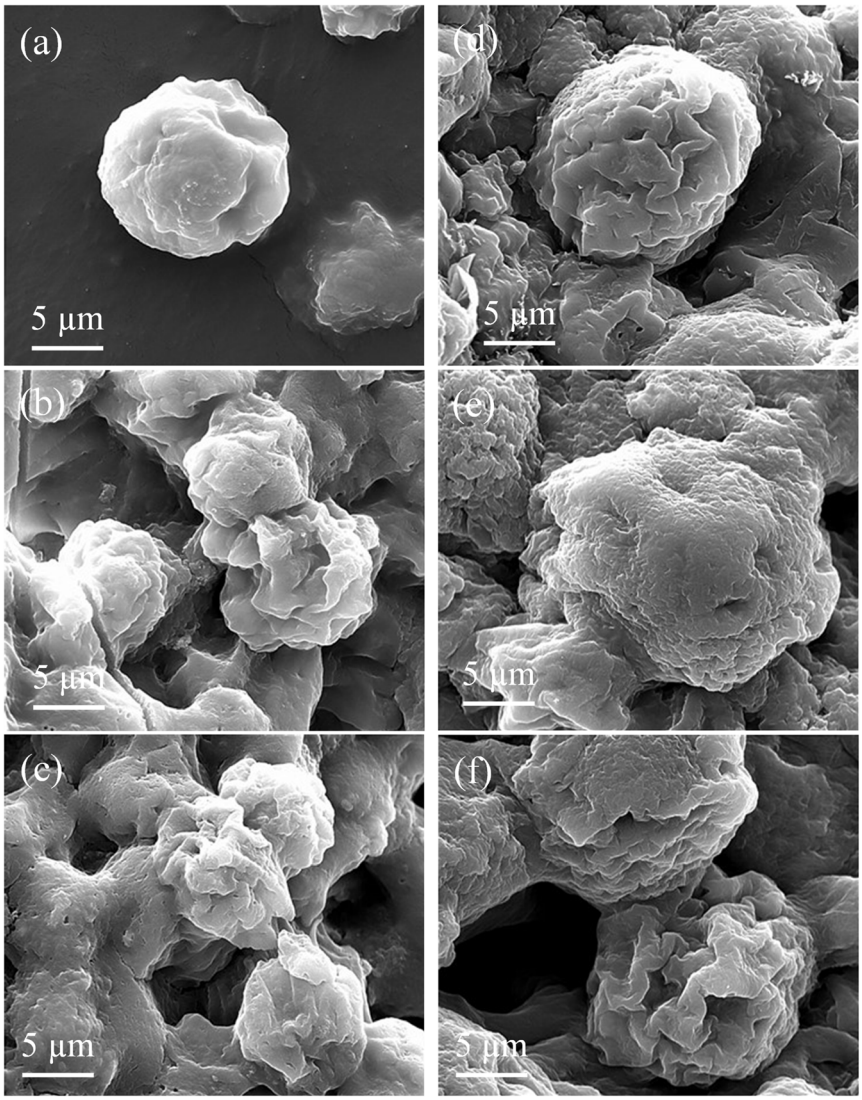


Fig. 10 SEM images of control and treated HCT-116 cells (left panel) and HEK-293 cells (right panel). (a and d) Control cells, (b and e) treated with 60 μg $mL^{-1}$ AuNPs@GA for 24 h, and (c and f) treated with 60 μg $mL^{-1}$ AuNPs@CNM for 24 h. All scale bars are 5 μm.

observation made by light microscopy on ultramicrotomy-prepared cells.

### 3.4 Apoptotic study of AuNPs using DAPI staining

DAPI was utilized to obtain additional information about the cytotoxicity of treatments on cancer cell DNA. DAPI is a blue stain where a fluorescent stain is used to differentiate between live and dead cells. It counts cells, measures apoptosis, identifies cell status based on DNA state, and examines nuclear morphological changes. The treatment of AuNPs@GA and AuNPs@CNM induced a remarkable reduction in colon cancer cells. According to Fig. 11, the DAPI-stained cell number was notably reduced in AuNPs@GA and AuNPs@CNM treated cells compared to control cells. Additionally, it was detected that AuNPs@GA and AuNPs@CNM-treated cells exhibited some changes in cell morphology, such as the shrinking of the cells, indicating the formation of apoptotic bodies. These results demonstrate the inhibition of HCT-116 growth by inducing apoptosis.

## 4 Endocytosis triggered apoptotic mechanism

Apoptosis, or programmed cell death, is a controlled process essential for maintaining cellular homeostasis and development. NPs characterized by nanoscale dimensions have attracted significant interest in biological applications, and they are actively taken up by the cell through various endocytic pathways. In addition, due to their effective uptake, engineered NPs are suggested to enhance the cellular permeability of tiny molecules and proteins.[78] Cellular uptake (endocytosis) of NPs involves complex processes and biomolecular interactions that facilitate the NPs in crossing the plasma membrane. The capacity for the uptake is attributed to the large and highly

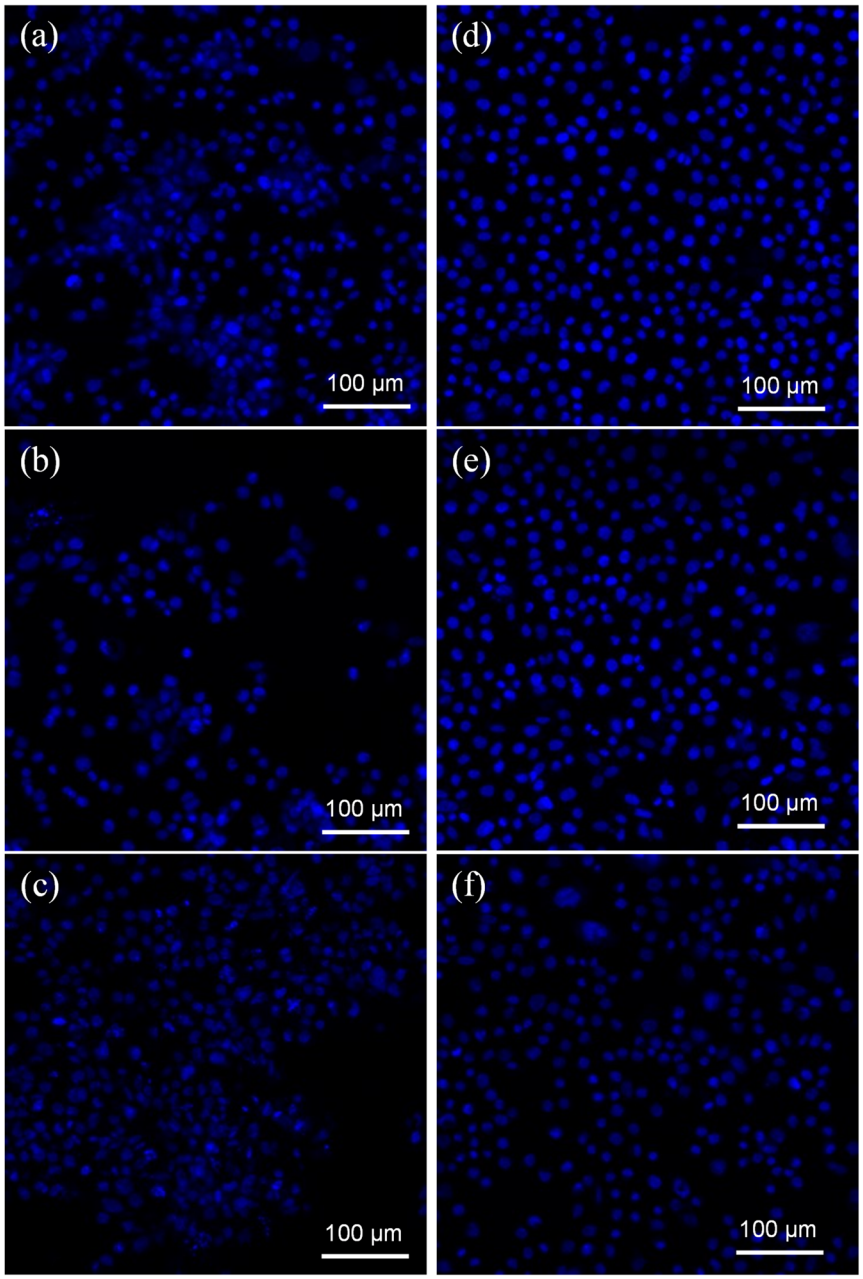


Fig. 11 Confocal microscopy images of HCT-116 cells stained with DAPI: (a) control cells; treated with (b) 60 μg $mL^{-1}$ AuNPs@GA, and (c) 60 μg $mL^{-1}$ AuNPs@CNM. Confocal microscopy images of HEK-293 stained with DAPI: (d) control cells; treated with (e) 60 μg $mL^{-1}$ AuNPs@GA and (f) 60 μg $mL^{-1}$ AuNPs@CNM.

energetic surface area of NPs which allows them to interact with biomolecules, including those that constitute the cell membrane.[79] The plasma membrane (a thin layer) separates intracellular components of the cell from the external environment and is composed of lipids and proteins. NPs can enter the cells through several pathways, *e.g.*, endocytosis-based uptake and direct cellular entry. These pathways are crucial for optimizing NP design and functionality. Depending on their size, surface charge, and coating, there are several primary mechanisms of endocytosis, such as clathrin-mediated endocytosis, caveolin-mediated endocytosis, clathrin/caveolae-independent endocytosis, and macropinocytosis.[80,81] In endocytosis, the AuNPs enter the cells and are encapsulated into vesicles known as endosomes. These endosomes can progress to late endosomes or lysosomes, in which the internal environment becomes highly acidic. AuNPs are then escaped from the endosomal compartments to reach their target inside the cell, suggesting that at least some AuNPs evade the lysosomal pathway. Thereby releasing NPs to the cytoplasm cytosol and then interact with cellular organelles or cytoskeleton components.[82] Some NPs may exit from the cell *via* exocytosis, or accumulate in their target organ or tissue, *i.e.*, localized in the nucleus and mitochondria. This process leads to membrane

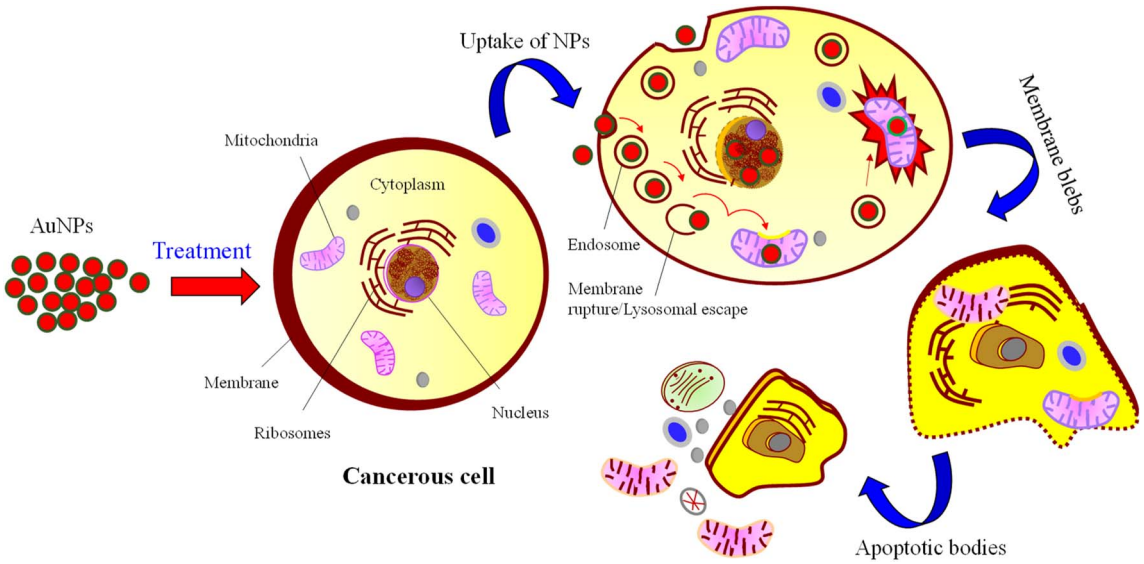


Fig. 12 Main features of the apoptotic cell death that are exploited for cytotoxicity assays. NPs conjugates (AuNPs@GA or AuNPs@CNM) are directed to the cell upon treatment, causing partial rupture of the outer mitochondrial membrane as well as nuclear membrane, triggering cell death.

blebbing and consequently breaks apart the cell into several apoptotic bodies as illustrated in the schematic Fig. 12.[83]

## 5 Conclusion

Due to their natural and biocompatible properties, GA and CNM extracts were effectively employed for the synthesis of AuNPs. The structural and morphological characteristics of the two types of NPs (AuNPs@GA and AuNPs@CNM) were evaluated through various characterization techniques. TEM analysis revealed that AuNPs@GA predominantly exhibited a spherical shape with an average diameter of approximately 12 nm, while AuNPs@CNM displayed diverse shapes, including spherical, hexagonal, and diamond, with an average diameter of around 17 nm. UV-Vis spectroscopy confirmed the successful synthesis of AuNPs, with absorption peaks at 520–530 nm. The synthesized AuNPs@GA and AuNPs@CNM demonstrated significant anticancer activities against HCT-116 colorectal cancer cells, while exhibiting minimal cytotoxic effects on HEK-293 cells, indicating a level of selectivity. The inhibitory action on HCT-116 cancer cells was quantified with $IC_{50}$ values of 9.14 and 11.76 μg $mL^{-1}$ for AuNPs@GA and AuNPs@CNM, respectively. Furthermore, the treatment with AuNPs@GA and AuNPs@CNM induced observable signs of apoptosis and cell death, as confirmed by light and confocal microscopies. These findings highlight the potential of these synthesized AuNPs as effective agents for cancer treatment, demonstrating both cytotoxicity against cancer cells and biocompatibility with normal cells. The use of natural extracts in the synthesis process adds an eco-friendly dimension to the potential applications of NPs in cancer therapy.

## Consent for publication

This manuscript is approved by all authors for submission.

## Data availability

The data supporting this article have been included in the main article.

## Author contributions

The manuscript was written through the contribution of all authors. All authors have provided approval to the final version of the manuscript. Sultan Akhtar: methodology, investigation, data curation and data analysis, writing – original draft. Fatimah Zuhair: methodology, investigation, data curation, writing – original draft. M. Nawaz: investigation, writing – review and editing. F. A. Khan: data analysis, writing – review and editing.

## Conflicts of interest

The authors declare that they have no competing interests.

## Acknowledgements

The authors are acknowledged Institute for Research and Medical Consultations (IRMC), Imam Abdulrahman Bin Faisal University, Dammam, Saudi Arabia for providing the lab facilities. Mr Edwardson to help with SEM/TEM sample preparation, Mr Dionecio Jr. Bagon Dela Roca are acknowledged for assisting in cell culture-related work.

## References

1 K. Bukowski, M. Kciuk and R. Kontek, Mechanisms of Multidrug Resistance in Cancer Chemotherapy, *Int. J. Mol. Sci.*, 2020, **21**(9), 3233, https://www.ncbi.nlm.nih.gov/pmc/articles/PMC7247559/.

2 P. Kuppusamy, S. J. A. Ichwan, P. N. H. Al-Zikri, W. H. Suriyah, I. Soundharrajan, N. Govindan, *et al.*, In Vitro Anticancer Activity of Au, Ag Nanoparticles Synthesized Using Commelina nudiflora L. Aqueous Extract Against HCT-116 Colon Cancer Cells, *Biol. Trace Elem. Res.*, 2016, **173**(2), 297–305, https://link.springer.com/10.1007/s12011-016-0666-7.

3 R. Seigneuric, L. Markey, D. S. A. Nuyten, C. Dubernet, C. T. A. Evelo, E. Finot, *et al.*, From nanotechnology to nanomedicine: applications to cancer research, *Curr. Mol. Med.*, 2010, **10**(7), 640–652.

4 P. D. Violette and F. Saad, Chemoprevention of Prostate Cancer: Myths and Realities, *J. Am. Board Fam. Med.*, 2012, **25**(1), 111–119, https://www.jabfm.org/content/25/1/111.

5 R. B. Liszbinski, G. G. Romagnoli, C. M. Gorgulho, C. R. Basso, V. A. Pedrosa and R. Kaneno, Anti-EGFR-Coated Gold Nanoparticles In Vitro Carry 5-Fluorouracil to Colorectal Cancer Cells, *Mater.*, 2020, **13**(2), E375, https://europepmc.org/articles/PMC7013715.

6 K. M. Augestad, M. A. Merok and D. Ignatovic, Tailored Treatment of Colorectal Cancer: Surgical, Molecular, and Genetic Considerations, *Clin. Med. Insights: Oncol.*, 2017, **11**, 1179554917690766, https://www.ncbi.nlm.nih.gov/pmc/articles/PMC5395262/.

7 J. Mishra, J. Drummond, S. H. Quazi, S. S. Karanki, J. J. Shaw, B. Chen, *et al.*, Prospective of colon cancer treatments and scope for combinatorial approach to enhanced cancer cell apoptosis, *Crit. Rev. Oncol. Hematol.*, 2013, **86**(3), 232–250, https://linkinghub.elsevier.com/retrieve/pii/S1040842812001977.

8 A. Fouda, A. M. Eid, E. Guibal, M. F. Hamza, S. E. D. Hassan, D. H. M. Alkhalifah, *et al.*, Green Synthesis of Gold Nanoparticles by Aqueous Extract of Zingiber officinale: Characterization and Insight into Antimicrobial, Antioxidant, and In Vitro Cytotoxic Activities, *Appl. Sci.*, 2022, **12**(24), 12879, https://www.mdpi.com/2076-3417/12/24/12879.

9 H. Wen, H. Jung and X. Li, Drug Delivery Approaches in Addressing Clinical Pharmacology-Related Issues: Opportunities and Challenges, *AAPS J.*, 2015, **17**(6), 1327–1340.

10 Y. Xin, M. Yin, L. Zhao, F. Meng and L. Luo, Recent progress on nanoparticle-based drug delivery systems for cancer therapy, *Cancer Biol. Med.*, 2017, **14**(3), 228–241, https://www.ncbi.nlm.nih.gov/pmc/articles/PMC5570600/.

11 E. A. Murphy, B. K. Majeti, L. A. Barnes, M. Makale, S. M. Weis, K. Lutu-Fuga, *et al.*, Nanoparticle-mediated drug delivery to tumor vasculature suppresses metastasis, *Proc. Natl. Acad. Sci.*, 2008, **105**(27), 9343–9348, https://www.pnas.org/doi/10.1073/pnas.0803728105.

12 N. Patil, R. Bhaskar, V. Vyavhare, R. Dhadge, V. Khaire and Y. Patil, Overview on Methods of Synthesis of Nanoparticles, *Int. J. Curr. Pharm. Res.*, 2021, **15**, 11–16.

13 S. Hiremath, M. Chandraprabha, M. Antonyraj, I. V. Gopal, A. Y. Jain, K. Bansal. Green synthesis of ZnO nanoparticles by Calotropis Gigantea, 2013, https://www.semanticscholar.org/paper/Green-synthesis-of-ZnO-nanoparticles-by-Calotropis-Hiremath-Chandraprabha/64c832c744a29cf141589bb2c54125c4ffec98ad.

14 V. V. Makarov, A. J. Love, O. V. Sinitsyna, S. S. Makarova, I. V. Yaminsky, M. E. Taliansky, *et al.*, "Green" nanotechnologies: synthesis of metal nanoparticles using plants, *Acta Naturae*, 2014, **6**(1), 35–44.

15 P. G. Jamkhande, N. W. Ghule, A. H. Bamer and M. G. Kalaskar, Metal nanoparticles synthesis: An overview on methods of preparation, advantages and disadvantages, and applications, *J. Drug Delivery Sci. Technol.*, 2019, **53**, 101174, https://www.sciencedirect.com/science/article/pii/S1773224718308189.

16 X. Chen, X. Zhao and G. Wang, Review on marine carbohydrate-based gold nanoparticles represented by alginate and chitosan for biomedical application, *Carbohydr. Polym.*, 2020, **244**, 116311.

17 M. Jannathul Firdhouse and P. Lalitha, Biogenic green synthesis of gold nanoparticles and their applications – A review of promising properties, *Inorg. Chem. Commun.*, 2022, **143**, 109800, https://www.sciencedirect.com/science/article/pii/S1387700322006086.

18 M. G. Heinemann, C. H. Rosa, G. R. Rosa and D. Dias, Biogenic synthesis of gold and silver nanoparticles used in environmental applications: A review, *Trends Environ. Anal. Chem.*, 2021, **30**, e00129, https://www.sciencedirect.com/science/article/pii/S2214158821000167.

19 A. K. Adhikari and K. S. Lin, Synthesis, fine structural characterization, and CO2 adsorption capacity of metal organic frameworks-74, *J. Nanosci. Nanotechnol.*, 2014, **14**(4), 2709–2717.

20 N. Farhadian, R. Usefi Mashoof, S. Khanizadeh, E. Ghaderi, M. Farhadian and A. Miresmaeili, Streptococcus mutans counts in patients wearing removable retainers with silver nanoparticles vs those wearing conventional retainers: A randomized clinical trial, *Am. J. Orthod. Dentofac. Orthop. Off. Publ. Am. Assoc. Orthod. Its Const. Soc. Am. Board Orthod.*, 2016, **149**(2), 155–160.

21 M. A. Huq, M. Ashrafudoulla, M. M. Rahman, S. R. Balusamy and S. Akter, Green Synthesis and Potential Antibacterial Applications of Bioactive Silver Nanoparticles: A Review, *Polymers*, 2022, **14**(4), 742.

22 M. A. Huq and S. Akter, Characterization and Genome Analysis of Arthrobacter bangladeshi sp. nov., Applied for the Green Synthesis of Silver Nanoparticles and Their Antibacterial Efficacy against Drug-Resistant Human Pathogens, *Pharmaceutics*, 2021, **13**(10), 1691.

23 P. Singh, Y. J. Kim, H. Singh, C. Wang, K. H. Hwang, M. E. A. Farh, *et al.*, Biosynthesis, characterization, and antimicrobial applications of silver nanoparticles, *Int. J. Nanomed.*, 2015, **10**, 2567–2577.

24 P. Singh and I. Mijakovic, Green synthesis and antibacterial applications of gold and silver nanoparticles from Ligustrum vulgare berries, *Sci. Rep.*, 2022, **12**(1), 7902.

25 H. Zazo, C. I. Colino and J. M. Lanao, Current applications of nanoparticles in infectious diseases, *J. Control Release*, 2016, **224**, 86–102.

26 S. A. Dahoumane, C. Jeffryes, M. Mechouet and S. N. Agathos, Biosynthesis of Inorganic Nanoparticles: A Fresh Look at the Control of Shape, Size and Composition, *Bioeng.*, 2017, **4**(1), 14.

27 Y. Ghosn, M. H. Kamareddine, A. Tawk, C. Elia, A. El Mahmoud, K. Terro, *et al.*, Inorganic Nanoparticles as Drug Delivery Systems and Their Potential Role in the Treatment of Chronic Myelogenous Leukaemia, *Technol. Cancer Res. Treat.*, 2019, **18**, 1533033819853241.

28 K. Golchin, J. Golchin, S. Ghaderi, N. Alidadiani, S. Eslamkhah, M. Eslamkhah, *et al.*, Gold nanoparticles applications: from artificial enzyme till drug delivery, *Artif. Cells, Nanomed., Biotechnol.*, 2018, **46**(2), 250–254.

29 X. Han, X. Jiang, L. Guo, Y. Wang, V. P. Veeraraghavan, S. Krishna Mohan, *et al.*, Anticarcinogenic potential of gold nanoparticles synthesized from Trichosanthes kirilowii in colon cancer cells through the induction of apoptotic pathway, *Artif. Cells, Nanomed., Biotechnol.*, 2019, **47**(1), 3577–3584.

30 S. Jeyarani, N. M. Vinita, P. Puja, S. Senthamilselvi, U. Devan, A. J. Velangani, *et al.*, Biomimetic gold nanoparticles for its cytotoxicity and biocompatibility evidenced by fluorescence-based assays in cancer (MDA-MB-231) and non-cancerous (HEK-293) cells, *J. Photochem. Photobiol., B*, 2020, **202**, 111715.

31 P. M. Tiwari, K. Vig, V. A. Dennis and S. R. Singh, Functionalized Gold Nanoparticles and Their Biomedical Applications, *Nanomater.*, 2011, **1**(1), 31–63.

32 A. M. Gamal-Eldeen, D. Moustafa, S. M. El-Daly, M. A. M. Abo-Zeid, S. Saleh, M. Khoobchandani, *et al.*, Gum Arabic-encapsulated gold nanoparticles for a non-invasive photothermal ablation of lung tumor in mice, *Biomed. Pharmacother.*, 2017, **89**, 1045–1054.

33 X. Li, H. Y. Lu, X. W. Jiang, Y. Yang, B. Xing, D. Yao, *et al.*, Cinnamomum cassia extract promotes thermogenesis during exposure to cold via activation of brown adipose tissue, *J. Ethnopharmacol.*, 2021, **266**, 113413.

34 E. Mzwd, N. M. Ahmed, N. Suradi, S. K. Alsaee, A. S. Altowyan, M. A. Almessiere, *et al.*, Green synthesis of gold nanoparticles in Gum Arabic using pulsed laser ablation for CT imaging, *Sci. Rep.*, 2022, **12**(1), 10549.

35 N. A. AlMuslet, E. A. Hassan, A. S. A. E. M. Al-Sherbini and M. G. A. Muhgoub, Graft copolymerization of acrylamide onto gum karaya using diode laser (532nm), *Elixir Chem. Phys.*, 2011, 2227–2230.

36 H. R. de Barros, M. B. Cardoso, C. C. de Oliveira, C. R. C. Franco, D. L. de Belan, M. Vidotti, *et al.*, Stability of gum arabic-gold nanoparticles in physiological simulated pHs and their selective effect on cell lines, *RSC Adv.*, 2016, **6**(12), 9411–9420, **https://pubs.rsc.org/en/content/articlelanding/2016/ra/c5ra24858b**.

37 A. Abuarra, R. Hashim, S. Bauk, S. Kandaiya and E. T. Tousi, Fabrication and characterization of gum Arabic bonded Rhizophora spp. particleboards, *Mater. Des.*, 2014, **60**, 108–115, **https://www.sciencedirect.com/science/article/pii/S0261306914002258**.

38 C. C. Wu and D. H. Chen, Facile green synthesis of gold nanoparticles with gum arabic as a stabilizing agent and reducing agent, *Gold Bull.*, 2010, **43**(4), 234–240, **https://link.springer.com/10.1007/BF03214993**.

39 P. Iranpour, M. Ajamian, A. Safavi, N. Iranpoor, A. Abbaspour and S. Javanmardi, Synthesis of highly stable and biocompatible gold nanoparticles for use as a new X-ray contrast agent, *J. Mater. Sci.: Mater. Med.*, 2018, **29**(5), 48.

40 A. Alam, M. J. Ansari, M. H. Alqarni, M. A. Salkini and M. Raish, Antioxidant, Antibacterial, and Anticancer Activity of Ultrasonic Nanoemulsion of Cinnamomum Cassia L, *Essent. Oil Plants*, 2023, **12**(4), 834.

41 Y. P. Jia, B. Y. Ma, X. W. Wei and Z. Y. Qian, The in vitro and in vivo toxicity of gold nanoparticles, *Chin. Chem. Lett.*, 2017, **28**(4), 691–702, **https://www.sciencedirect.com/science/article/pii/S1001841717300438**.

42 S. Akhtar and S. Ali, Characterization of Nanomaterials: Techniques and Tools, In *Applications of Nanomaterials in Human Health*, ed. F. A. Khan. Springer, Singapore, 2020, pp. 23–43, DOI: **10.1007/978-981-15-4802-4_3**.

43 S. Akhtar, S. M. Asiri, F. A. Khan, S. T. Gunday, A. Iqbal, N. Alrushaid, *et al.*, Formulation of gold nanoparticles with hibiscus and curcumin extracts induced anti-cancer activity, *Arab. J. Chem.*, 2022, **15**(2), 103594, **https://www.sciencedirect.com/science/article/pii/S1878535221006092**.

44 S. Akhtar, S. Rehman, S. M. Asiri, F. A. Khan, U. Baig, A. S. Hakeem, *et al.*, Evaluation of bioactivities of zinc oxide, cadmium sulfide and cadmium sulfide loaded zinc oxide nanostructured materials prepared by nanosecond pulsed laser, *Mater. Sci. Eng. C*, 2020, **116**, 111156.

45 F. A. Khan, S. Akhtar, D. Almohazey, M. Alomari, S. A. Almofty and A. Eliassari, Fluorescent magnetic submicronic polymer (FMSP) nanoparticles induce cell death in human colorectal carcinoma cells, *Artif. Cells, Nanomed., Biotechnol.*, 2018, **46**(sup3), S247–S253.

46 N. R. S. Sibuyi, V. C. Thipe, K. Panjtan-Amiri, M. Meyer and K. V. Katti, Green synthesis of gold nanoparticles using Acai berry and Elderberry extracts and investigation of their effect on prostate and pancreatic cancer cells, *Nanobiomedicine*, 2021, **8**, 1849543521995310.

47 D. Goyal, A. Saini, G. S. S. Saini and R. Kumar, Green synthesis of anisotropic gold nanoparticles using cinnamon with superior antibacterial activity, *Mater. Res. Express*, 2019, **6**(7), 075043, DOI: **10.1088/2053-1591/ab15a6**.

48 S. K. Alsaee, N. M. Ahmed, E. Mzwd, A. F. Omar, A. I. Aljameel, N. Afzal, *et al.*, pH sensor based on AuNPs/ITO membrane as extended gate field-effect transistor, *Appl. Phys. B*, 2021, **128**(1), 3, DOI: **10.1007/s00340-021-07727-1**.

49 G. Oberdörster, E. Oberdörster and J. Oberdörster, Nanotoxicology: an emerging discipline evolving from studies of ultrafine particles, *Environ. Health Perspect.*, 2005, **113**(7), 823–839.

50 N. Pauzi, N. M. Zain and N. A. A. Yusof, Gum arabic as natural stabilizing agent in green synthesis of ZnO nanofluids for antibacterial application, *J. Environ. Chem.*

*Eng.*, 2020, **8**(3), 103331, https://www.sciencedirect.com/science/article/pii/S2213343719304543.

51 O. S. ElMitwalli, O. A. Barakat, R. M. Daoud, S. Akhtar and F. Z. Henari, Green synthesis of gold nanoparticles using cinnamon bark extract, characterization, and fluorescence activity in Au/eosin Y assemblies, *J. Nanopart. Res.*, 2020, **22**(10), 309, DOI: 10.1007/s11051-020-04983-8.

52 H. Ribeiro de Barros, M. B. Cardoso, C. Camargo de Oliveira, C. R. Cavichiolo Franco, D. de Lima Bellan, M. Vidotti, *et al.*, Correction: Stability of gum Arabic-gold nanoparticles in physiological simulated pHs and their selective effect on cell lines, *RSC Adv.*, 2018, **8**(71), 40596.

53 U. Gaware, V. Kamble and B. Ankamwar, Ecofriendly Synthesis of Anisotropic Gold Nanoparticles: A Potential Candidate of SERS Studies, *Int. J. Electrochem.*, 2012, e276246, https://www.hindawi.com/journals/ijelc/2012/276246/.

54 H. Palza, Antimicrobial polymers with metal nanoparticles, *Int. J. Mol. Sci.*, 2015, **16**(1), 2099–2116.

55 A. Madhusudhan, G. B. Reddy and I. M. Krishana, Green Synthesis of Gold Nanoparticles by Using Natural Gums. In *Nanomaterials and Plant Potential*, ed. A. Husen and M. Iqbal, Springer International Publishing, Cham, 2019, pp. 111–134, DOI: 10.1007/978-3-030-05569-1_4.

56 M. Luty-Błocho, J. Cyndrowska, B. Rutkowski and V. Hessel, Synthesis of Gold Clusters and Nanoparticles Using Cinnamon Extract-A Mechanism and Kinetics Study, *Molecules*, 2024, **29**(7), 1426, https://pubmed.ncbi.nlm.nih.gov/38611706/.

57 F. Qureshi, M. Nawaz, M. A. Ansari, F. A. Khan, M. M. Berekaa, S. A. Abubshait, *et al.*, Synthesis of M-Ag3PO4, (M = Se, Ag, Ta) Nanoparticles and Their Antibacterial and Cytotoxicity Study, *Int. J. Mol. Sci.*, 2022, **23**(19), 11403.

58 M. Eskandari-Nojehdehi, H. Jafarizadeh-Malmiri and A. Jafarizad, Microwave Accelerated Green Synthesis of Gold Nanoparticles Using Gum Arabic and their Physico-Chemical Properties Assessments, *Z. Phys. Chem.*, 2018, **232**(3), 325–343, https://www.degruyter.com/document/doi/10.1515/zpch-2017-1001/html?lang=en.

59 P. Renuga Devi, C. Senthil Kumar, P. Selvamani, N. Subramanian and K. Ruckmani, Synthesis and characterization of Arabic gum capped gold nanoparticles for tumor-targeted drug delivery, *Mater. Lett.*, 2015, **139**, 241–244, https://www.sciencedirect.com/science/article/pii/S0167577X14017972.

60 R. Sankar, P. K. S. M. Rahman, K. Varunkumar, C. Anusha, A. Kalaiarasi, K. S. Shivashangari, *et al.*, Facile synthesis of *Curcuma longa* tuber powder engineered metal nanoparticles for bioimaging applications, *J. Mol. Struct.*, 2017, **1129**, 8–16, https://www.sciencedirect.com/science/article/pii/S0022286016309814.

61 D. Pooja, S. Panyaram, H. Kulhari, S. S. Rachamalla and R. Sistla, Xanthan gum stabilized gold nanoparticles: Characterization, biocompatibility, stability and cytotoxicity, *Carbohydr. Polym.*, 2014, **110**, 1–9, https://www.sciencedirect.com/science/article/pii/S0144861714002732.

62 S. K. Surapaneni, S. Bashir and K. Tikoo, Gold nanoparticles-induced cytotoxicity in triple negative breast cancer involves different epigenetic alterations depending upon the surface charge, *Sci. Rep.*, 2018, **8**(1), 12295, https://www.nature.com/articles/s41598-018-30541-3.

63 S. Akhtar, S. M. Asiri, F. A. Khan, S. T. Gunday, A. Iqbal, N. Alrushaid, *et al.*, Formulation of gold nanoparticles with hibiscus and curcumin extracts induced anti-cancer activity, *Arab. J. Chem.*, 2021, **15**, 103594.

64 H. Malaikolundhan, G. Mookkan, G. Krishnamoorthi, N. Matheswaran, M. Alsawalha, V. P. Veeraraghavan, *et al.*, Anticarcinogenic effect of gold nanoparticles synthesized from Albizia lebbeck on HCT-116 colon cancer cell lines, *Artif. Cells, Nanomed., Biotechnol.*, 2020, **48**(1), 1206–1213, DOI: 10.1080/21691401.2020.1814313.

65 H. M. Aldawsari, S. Singh, N. A. Alhakamy, R. B. Bakhaidar, A. A. Halwani and S. M. Badr-Eldin, Gum Acacia Functionalized Colloidal Gold Nanoparticles of Letrozole as Biocompatible Drug Delivery Carrier for Treatment of Breast Cancer, *Pharmaceutics*, 2021, **13**(10), 1554, https://www.ncbi.nlm.nih.gov/pmc/articles/PMC8538880/.

66 O. M. El-Borady, M. S. Ayat, M. A. Shabrawy and P. Millet, Green synthesis of gold nanoparticles using Parsley leaves extract and their applications as an alternative catalytic, antioxidant, anticancer, and antibacterial agents, *Adv. Powder Technol.*, 2020, **31**(10), 4390–4400, https://www.sciencedirect.com/science/article/pii/S0921883120304362.

67 S. C. E. González, E. Bolaina-Lorenzo, J. J. Pérez-Trujillo, B. A. Puente-Urbina, O. Rodríguez-Fernández, A. Fonseca-García, *et al.*, Antibacterial and anticancer activity of ZnO with different morphologies: a comparative study, *3 Biotech.*, 2021, **11**(2), 68.

68 V. Labhasetwar, C. Song, W. Humphrey, R. Shebuski and R. J. Levy, Arterial uptake of biodegradable nanoparticles: effect of surface modifications, *J. Pharm. Sci.*, 1998, **87**(10), 1229–1234.

69 K. P. Steckiewicz, E. Barcinska, A. Malankowska, A. Zauszkiewicz-Pawlak, G. Nowaczyk, A. Zaleska-Medynska, *et al.*, Impact of gold nanoparticles shape on their cytotoxicity against human osteoblast and osteosarcoma in in vitro model. Evaluation of the safety of use and anti-cancer potential, *J. Mater. Sci.: Mater. Med.*, 2019, **30**(2), 22.

70 C. Contini, J. W. Hindley, T. J. Macdonald, J. D. Barritt, O. Ces and N. Quirke, Size dependency of gold nanoparticles interacting with model membranes, *Commun. Chem.*, 2020, **3**(1), 130, https://www.mendeley.com/catalogue/e80f24ad-fa8b-32cc-84fd-bd80025d0f31/.

71 E. Shahhoseini, M. Nakayama, V. Panettieri, C. Hall, B. Feltise and M. Gesoa, Effects of synchrotron-based X-rays and gold nanoparticles on normal and cancer cell morphology and migration, *J. Synchrotron Radiat.*, 2023,

**30**(Pt 2), 359–367, https://pubmed.ncbi.nlm.nih.gov/36891849/.

72 X. J. Mi, H. R. Park, S. Dhandapani, S. Lee and Y. J. Kim, Biologically synthesis of gold nanoparticles using Cirsium japonicum var. maackii extract and the study of anti-cancer properties on AGS gastric cancer cells, *Int. J. Biol. Sci.*, 2022, **18**(15), 5809–5826.

73 M. N. Bin-Jumah, M. Al-Abdan, G. Al-Basher and S. Alarifi, Molecular Mechanism of Cytotoxicity, Genotoxicity, and Anticancer Potential of Green Gold Nanoparticles on Human Liver Normal and Cancerous Cells, *Dose-Response*, 2020, **18**(2), 1559325820912154.

74 M. Musielak, A. Boś-Liedke, I. Piotrowski, M. Kozak and W. Suchorska, The Role of Gold Nanorods in the Response of Prostate Cancer and Normal Prostate Cells to Ionizing Radiation-In Vitro Model, *Int. J. Mol. Sci.*, 2020, **22**(1), 16.

75 A. Fouda, A. M. Eid, M. A. Abdel-Rahman, E. F. El-Belely, M. A. Awad, S. E. D. Hassan, *et al.*, Enhanced Antimicrobial, Cytotoxicity, Larvicidal, and Repellence Activities of Brown Algae, Cystoseira crinita-Mediated Green Synthesis of Magnesium Oxide Nanoparticles, *Front. Bioeng. Biotechnol.*, 2022, **10**, 849921.

76 S. K. Verma, K. Nisha, P. K. Panda, P. Patel, P. Kumari, M. A. Mallick, *et al.*, Green synthesized MgO nanoparticles infer biocompatibility by reducing in vivo molecular nanotoxicity in embryonic zebrafish through arginine interaction elicited apoptosis, *Sci. Total Environ.*, 2020, **713**, 136521, https://www.sciencedirect.com/science/article/pii/S0048969720300310.

77 M. M. Mkandawire, M. Lakatos, A. Springer, A. Clemens, D. Appelhans, U. Krause-Buchholz, *et al.*, Induction of apoptosis in human cancer cells by targeting mitochondria with gold nanoparticles, *Nanoscale*, 2015, **7**(24), 10634–10640.

78 T. Sun, Y. S. Zhang, B. Pang, D. C. Hyun, M. Yang and Y. Xia, Engineered nanoparticles for drug delivery in cancer therapy, *Angew. Chem., Int. Ed.*, 2014, **53**(46), 12320–12364, https://pubmed.ncbi.nlm.nih.gov/25294565/.

79 P. Foroozandeh and A. A. Aziz, Insight into Cellular Uptake and Intracellular Trafficking of Nanoparticles, *Nanoscale Res. Lett.*, 2018, **13**(1), 339, DOI: 10.1186/s11671-018-2728-6.

80 M. S. de Almeida, E. Susnik, B. Drasler, P. Taladriz-Blanco, A. Petri-Fink and B. Rothen-Rutishauser, Understanding nanoparticle endocytosis to improve targeting strategies in nanomedicine, *Chem. Soc. Rev.*, 2021, **50**(9), 5397–5434, https://pubs.rsc.org/en/content/articlelanding/2021/cs/d0cs01127d.

81 E. Okoampah, Y. Mao, S. Yang, S. Sun and C. Zhou, Gold nanoparticles–biomembrane interactions: From fundamental to simulation, *Colloids Surf., B*, 2020, **196**, 111312, https://www.sciencedirect.com/science/article/pii/S0927776520306688.

82 M. Alle, G. Sharma, S. H. Lee and J. C. Kim, Next-generation engineered nanogold for multimodal cancer therapy and imaging: a clinical perspectives, *J. Nanobiotechnol.*, 2022, **20**(1), 222.

83 S. Behzadi, V. Serpooshan, W. Tao, M. A. Hamaly, M. Y. Alkawareek, E. C. Dreaden, *et al.*, Cellular Uptake of Nanoparticles: Journey Inside the Cell, *Chem. Soc. Rev.*, 2017, **46**(14), 4218–4244, https://www.ncbi.nlm.nih.gov/pmc/articles/PMC5593313/.